Journal of Power Sources 191 (2009) 614–618

Contents lists available at ScienceDirect

Journal of Power Sources

journal homepage: www.elsevier.com/locate/jpowsour

Short communication

Preparation and electrochemical properties of TiO_2 hollow spheres as an anode material for lithium-ion batteries

Jipeng Wang[a], Ying Bai[a], Muying Wu[b], Jiang Yin[c], W.F. Zhang[a,*]

[a] School of Physics & Electronics, Henan University, Minglun Str., Kaifeng 475001, China
[b] Department of Electronic Engineering, Dongguan University of Technology, Dongguan 523808, China
[c] National Laboratory of Solid State Microstructures, Nanjing University, Nanjing 210093, China

ARTICLE INFO

Article history:
Received 19 October 2008
Received in revised form 21 December 2008
Accepted 19 February 2009
Available online 4 March 2009

Keywords:
TiO_2
Hollow spheres
Electrochemistry
Li-ion batteries

ABSTRACT

TiO_2 hollow spheres are fabricated by a sol–gel process using carbon spheres as template. The diameter and the shell thickness of the TiO_2 hollow spheres are about 400–600 nm and 60–80 nm, respectively. The electrochemical properties of the hollow spheres are investigated by galvanostatic cycling and cyclic voltammetry (CV) measurements. The initial discharge capacity reaches 291.2 mAh g^{-1} at a current density of 60 mA g^{-1}. The average discharge capacity loss is about 1.72 mAh g^{-1} per cycle from the 2nd to the 40th cycles and the coulombic efficiency is approximately 98% after 40 cycles, indicating excellent cycling stability and reversibility.

1. Introduction

The demand for rechargeable batteries is increasing in power sources both of portable electronic equipments and automobile electrical systems. Among various candidate power systems, Li-ion batteries have attracted much attention because of their high energy storage density, long cycle life, little memory effect, poisonous metals free and so on [1,2]. To fabricate better Li-ion batteries, it is very important to explore novel materials for battery components, including cathode, anode and electrolyte. In the present commercial Li-ion batteries, graphite has been widely used as the intercalating anode for its high reversible capacity, even discharge/charge potential profile and low cost. However, graphite does have some disadvantages and cannot meet the performance requirements of some important applications satisfactorily, especially in the safety and rate performance [3]. To avoid these drawbacks, transition metal oxides such as WO_3, MoO_3 and TiO_2 have stimulated interest greatly [2,4,5]. Especially, titanium oxide is regarded as a promising active lithium intercalation material with high capacity, low-voltage (below ca. 2.0 V versus Li^+/Li) and low production cost.

A method to improve the electrochemical performance of Li-ion batteries is to increase the contact area between the active materials and electrolyte, hence making the Li^+ insertion/extraction more sufficiently [6]. For this purpose, keeping more porosity and less agglomeration of the active material through assembling them into three-dimensional architecture seems to be an effective way [6–8]. TiO_2 hollow spheres have been synthesized successfully by various methods, such as templating method [9], polymer-induced method [10], sol–gel method [11], hydrothermal method [12], etc. The most-applied method for the synthesis of hollow spheres is by far the templating of larger colloidal carbon spheres prepared by dehydrating glucose or sucrose under hydrothermal conditions. The surface of the carbon spheres have a distribution of –OH groups and –C=O groups, which makes surface modification unnecessary. The electrochemical properties of TiO_2 with varied morphologies, for instance, nanocrystallines [13], nanorods [14], nanotubes [15] and nanowires [16] have been studied by many previous researchers. However, the electrochemical features of TiO_2 hollow spheres have been reported rarely.

In this paper, we synthesized TiO_2 hollow spheres successfully by a sol–gel route using carbon spheres as template. This method is convenient, low cost and easily adaptable to mass production. The electrochemical properties were investigated by galvanostatic cycling and cyclic voltammetry.

2. Experimental

2.1. Preparation of TiO_2 hollow spheres

Carbon spheres with diameter about 1 μm were prepared by hydrothermal treatment of 1.0 M glucose aqueous solution in a

* Corresponding author. Tel.: +86 378 3881 940; fax: +86 378 3880 659.
E-mail addresses: wfzhang@henu.edu.cn, wfzhang6@163.com (W.F. Zhang).

0378-7753/$ – see front matter © 2009 Elsevier B.V. All rights reserved.
doi:10.1016/j.jpowsour.2009.02.056

teflon-lined autoclave at 190 °C for 16 h, according to the report of Sun and Li [17].

In a typical synthesis of TiO_2 hollow spheres, 6 ml $Ti(OC_4H_9)_4$ was dissolved slowly in 30 ml ethanol under constantly stirring to form the starting solution. Then the as-prepared carbon spheres (0.5 g) were added and well dispersed into the above solution. The mixture was kept at room temperature in a sealed beaker for 24 h with vigorous stirring before the products were collected by centrifugation. The products were washed with ethanol thoroughly to remove residual cations and anions, and then dried in air at 70 °C. The TiO_2 hollow spheres were obtained after annealing the dried powder at 500 °C in air for 3 h.

2.2. Structure and morphology characterization

X-ray diffraction (XRD, DX-2500, Fangyuan) measurement was performed on a diffractometer with Cu Kα radiation with λ = 1.54145 Å. The Raman spectrum was measured by a laser Raman Spectrometer (Renishaw-1000) at an output power of 100 mW of 457.5 nm solid-state laser. Scanning electron microscopy (SEM, JSM-5600LV, JEOL) and transmission electron microscopy (TEM, JEM-100cx, JEOL) were applied to examine the morphology.

2.3. Electrochemical characteristics

To prepare the working electrode, the TiO_2 hollow spheres, acetylene black (AB) and polyvinylidene fluoride (PVDF) binder were mixed together homogeneously in a weight ratio of 80:10:10, several drops of *N*-methylpymolidinone (NMP) was added until a slurry was obtained, the slurry was coated uniformly on a 10 μm thick copper foil. After drying at 120 °C for 24 h, a circular electrode with a diameter of 15 mm was punched from the copper foil and used as working electrode.

The simulated battery was assembled in a glove box filled with high-purity argon. The moisture content and oxygen level were less than 1 ppm inside the glove box. The TiO_2 hollow spheres as the working electrode and lithium foil was used as both the reference and counter electrodes. A solution of 1 M $LiPF_6$ dissolved in a mixture of ethylene carbonate (EC) and diethyl carbonate (DEC) (v/v = 1/1) was used as electrolyte and Celgard 2400 was used as separator membrane. The electrochemical measurements were performed using a three-electrode system at room temperature. The galvanostatic cycling was measured on a LAND cell test (Land-CT 2001A) system at a constant current density of 60 mA g^{-1} between 2.5 and 1.0 V. Cyclic voltammetry was performed on a CHI660B electrochemical workstation and recorded in the voltage range from 2.7 to 0.8 V at a scan rate of 0.2 mV s^{-1}.

3. Results and discussion

3.1. Physical characteristics

The SEM image of carbon spheres is shown in Fig. 1. It can be seen from the figure that the as-prepared carbon spheres is regular and smooth, with average diameter of 1 μm. Fig. 2 displays the XRD pattern of the TiO_2 hollow spheres after calcination at 500 °C using the as-prepared carbon spheres as template. It can be clearly seen that all of the diffraction peaks correspond to the pure anatase, which is in good agreement with JCPDS card 65-5714. The Raman spectrum of TiO_2 hollow spheres obtained at room temperature is plotted in Fig. 3. Raman peaks centered at ~140, 197, 395, 515 and 637 cm^{-1} are observed, which are consistent with the typical Raman features of anatase TiO_2 phase [15,18]. Fig. 4(a) and (b) illustrates the morphologies of the TiO_2 hollow spheres by SEM and TEM observations. It is apparent that the obtained products are interconnected hollow spheres with a size distribution from 400 to 600 nm, smaller than the original size of carbon spheres template. Some hollow spheres broken can be clearly observed from the SEM image. The shell thickness has a distribution of 60–80 nm according to the TEM image. To examine the stability of the hollow sphere

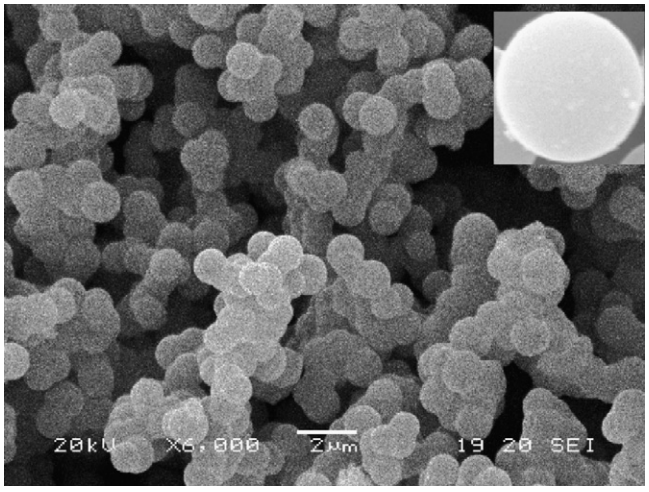

Fig. 1. SEM image of the carbon spheres.

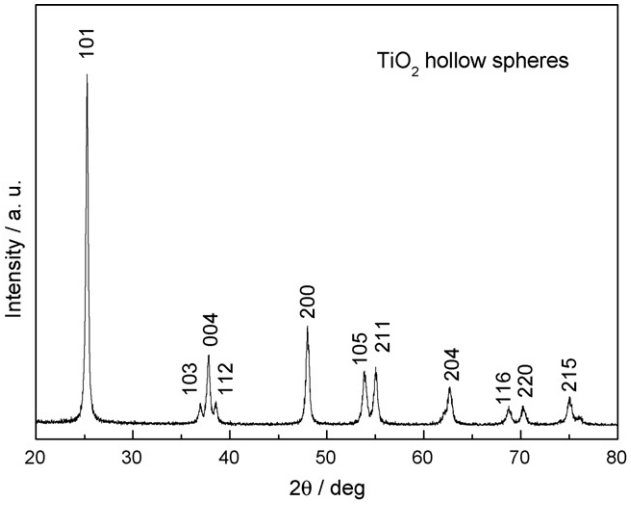

Fig. 2. XRD pattern of the TiO_2 hollow spheres.

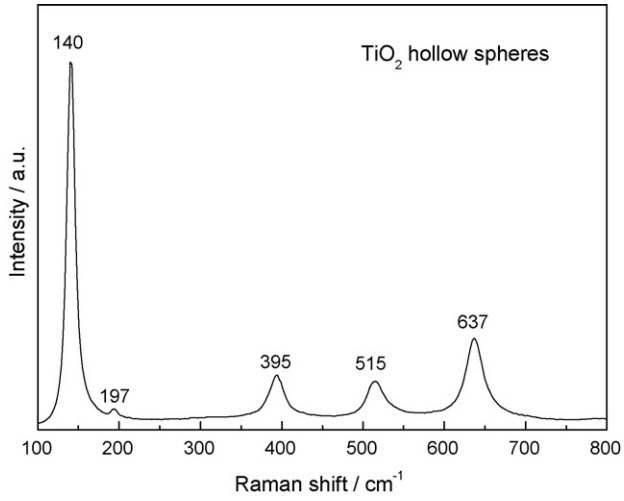

Fig. 3. Raman spectrum of the TiO_2 hollow spheres.

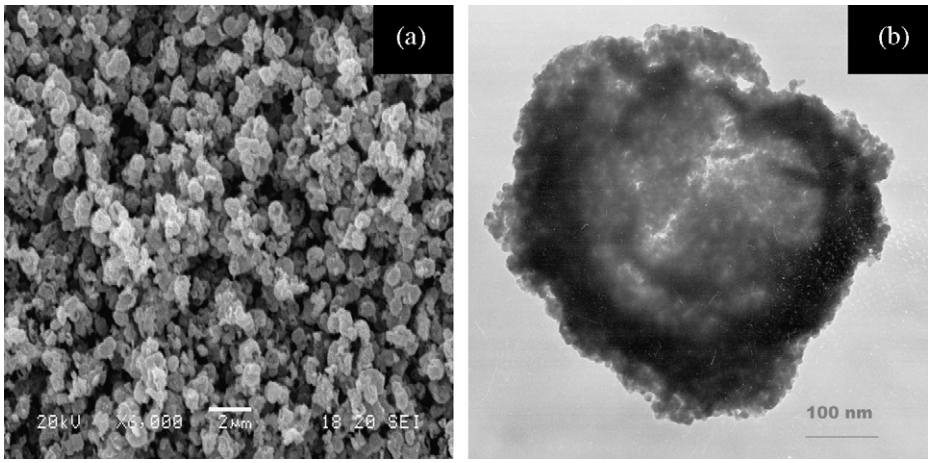

Fig. 4. SEM (a) and TEM (b) images of the TiO_2 hollow spheres.

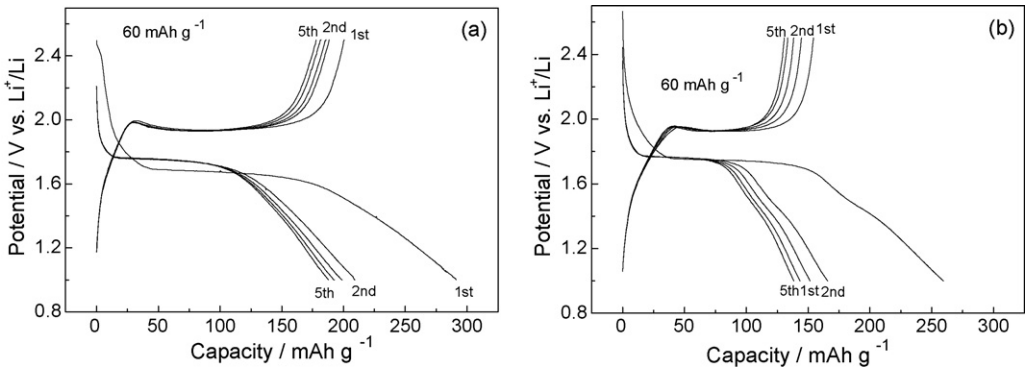

Fig. 5. Discharge/charge curves of the TiO_2 hollow sphere (a) and nano-TiO_2 particle (b) electrodes at a current density of 60 mA g^{-1}, and the voltage window is 1.0–2.5 V.

structure through electrode fabrication, the morphology of TiO_2-based electrode is also investigated by SEM (not shown). The SEM result demonstrates that the TiO_2 hollow spheres can well survive through the mixing and grinding steps, without broken during the fabrication of the electrode.

3.2. Electrochemical characteristics

Fig. 5(a) displays the initial five cycles of the TiO_2 hollow sphere electrode with cutoff voltages of 2.5–1.0 V (versus Li^+/Li) at a current density of 60 mA g^{-1}. In the first cycle, there are distinct discharge/charge potential plateaus at 1.75 and 1.94 V, respectively, which is consistent with the presence of predominant anatase as the starting materials [16,19]. The discharge curves can be divided into three domains. The first domain characterized by a monotonous potential decrease corresponds to a solid solution insertion mechanism [20]. The second domain characterized by a plateau at about 1.75 V is characteristic of a two-phase electrochemical reaction [21]. The Li^+ insertion/extraction reaction in TiO_2 hollow sphere electrode can be written as:

$$xLi^+ + xe^- + TiO_2 \leftrightarrow Li_xTiO_2 \quad (1)$$

where x is insertion coefficient, and it is usually close to 0.5 in anatase [22]. The third domain following the plateau is a further Li^+ inserting into $Li_{0.5}TiO_2$ process as the voltage drops linearly, which demonstrates that Li^+ inserting into $Li_{0.5}TiO_2$ can take place to a higher extent. It can be seen that most capacity is obtained between 2.0 and 1.0 V from the discharge/charge curves, higher discharge/charge voltage than that of graphite, hence improving the safety and stability of Li-ion batteries. To make a comparison with anatase TiO_2 nanoparticle electrodes, the nano-TiO_2 without addition of carbon spheres was prepared by the same sol–gel process and their electrochemical properties were also investigated by galvanostatic cycling. The initial five cycles of the nano-TiO_2 with cutoff voltages of 2.5–1.0 V (versus Li^+/Li) at a current density of 60 mA g^{-1} are displayed in Fig. 5(b). It can be seen from Fig. 5(b) that there are also distinct discharge/charge plateaus at 1.75 and 1.94 V for nano-TiO_2, which are characteristic lithiation/delithiation potentials for anatase material. The discharge curves in Fig. 5(b) can also be divided into three domains.

The cycling performance of the TiO_2 hollow sphere electrodes at a current density of 60 mA g^{-1} in the potential range of 2.5–1.0 V is displayed in Fig. 6(a). The cycling behavior of the nano-TiO_2 particle electrodes is also presented in Fig. 6(b) for a direct comparison. The

Table 1
Comparison of cycling performances of the *HSTO* and *NNTO* at the same condition.

Cycle number	Discharge capacity (mAh g^{-1}) (*HSTO*/*NNTO*)	Charge capacity (mAh g^{-1}) (*HSTO*/*NNTO*)	Coulombic efficiency (%) (*HSTO*/*NNTO*)
1	291.2/259.3	200.5/154.3	68.9/59.5
2	209.1/165.7	188.2/144.6	90.0/87.3
3	199.0/151.6	185.7/138.4	93.3/91.3
40	141.9/88.1	139.2/86.5	98.1/98.3

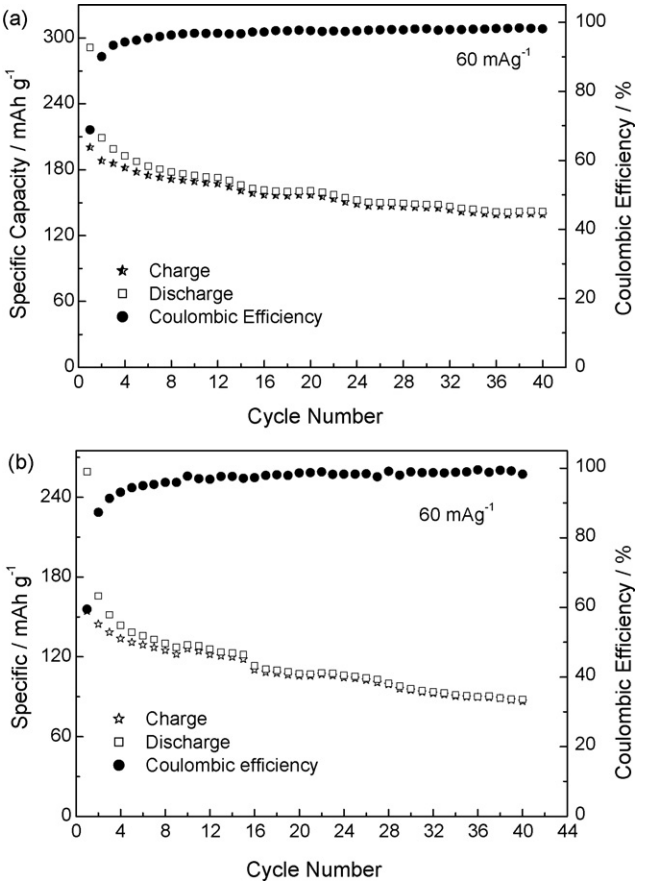

Fig. 6. Cycling performance of the TiO_2 hollow sphere (a) and nano-TiO_2 particle (b) electrodes at a current density of 60 mA g^{-1}, and the voltage window is 1.0–2.5 V.

more detailed comparison of the cycling performances of the TiO_2 hollow sphere (*HSTO*, for short) and nano-TiO_2 (*NNTO*) at the same condition is shown in Table 1. All these results indicate that the special structure of hollow spheres improves the capacity and cycling stability. The TiO_2 hollow spheres have a high initial discharge capacity of 291.2 mAh g^{-1}, with corresponding insertion coefficient 86.9%. It is believed that the high capacity of obtained sample should be attributed to the unique structure of hollow spheres. On one hand, most of the TiO_2 particles could be exposed to the electrolyte because of the unique structure of hollow spheres, reducing the Li^+ diffusion distance and increasing the contact area between TiO_2 and electrolyte greatly, and this can lead to a decrease of concentration polarization, thus the cycling performance improved naturally [23]. On the other hand, the primary grains of the TiO_2 hollow spheres can contact with AB (conducting assistant material) sufficiently, hence improving the electronic conductivity, and this may also help to improve the high rate performance. In addition, there are some extra site occupations of the hollow spheres for lithium insertion and the acetylene black and/or electrolyte decomposition in the TiO_2 hollow spheres may also contribute to the capacity [24]. The subsequent Li^+ extraction, proceeding up to 2.5 V, delivers a capacity of 200.5 mAh g^{-1}, with corresponding irreversible capacity 90.7 mAh g^{-1}. During discharge/charge cycles, the potential range was confined above 1.0 V. This should minimize the electrolyte reduction and hence any SEI layer formation. The trace water in the electrolyte could react irreversibly with lithium to form Li_2O, and this could be the major reason for the large irreversible capacity [16]. There is another explanation that the irreversible capacity is attributed to lithium intercalation into irreversible sites and side reactions [25].

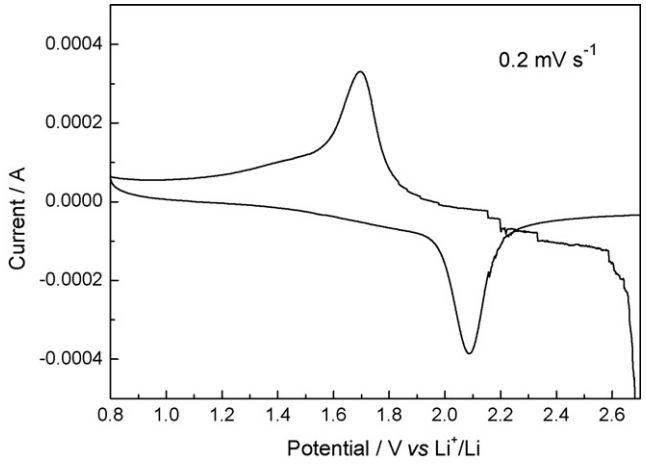

Fig. 7. Cyclic voltammetry of the TiO_2 hollow sphere electrode at a scan rate of 0.2 mV s^{-1} (voltage range: 0.8–2.7 V).

In the 2nd cycle, the discharge capacity reduces to 209.1 mAh g^{-1}, with a large discharge capacity fading (82 mAh g^{-1}) comparing with the first cycle. It can be seen from Fig. 5(a) that the discharge capacity decreases in every domain of the 2nd discharge curve compared with the 1st one. In the following cycles, the discharge capacity of the first and second domains scarcely changes, but the third domain decreases upon cycles, demonstrating the capacity decay mainly occurs in the third region. From the 2nd to the 40th cycles, the discharge capacity of TiO_2 hollow spheres decreases from 209.1 to 141.9 mAh g^{-1}, with a little average capacity fading of 1.72 mAh g^{-1} per cycle, showing better cycle performance comparing with the same morphology of TiO_2 as anode material reported by Chen et al. [18]. In their study, the discharge capacity of TiO_2 hollow microspheres decreases from 210 to 35 mAh g^{-1} from the 2nd to the 30th cycle, with a larger average capacity fading of 6.0 mAh g^{-1} per cycle, showing a poor cycling performance of the products, which was attributed to the relatively large structure strain during repeated lithium insertion and extraction processes. Based on Chen's work, the improved cycling performance in our study could be attributed to the smaller size of hollow cavity prepared by the sol–gel method, which is favorable in reducing the diffusion distance of lithium ions, and thus results in a much higher efficiency in the intercalation and extraction processes. After 40 cycles in our study, the coulombic efficiency reaches 98%, demonstrating that the discharge/charge tends to be stabilized and the coulombic efficiency increases upon cycles. It is believed that in the initial several cycles, the irreversible Li insertion sites are filled completely, the trace water is consumed gradually and the residual lithium in TiO_2 could improve the electric conductivity [26], thus, the irreversible capacity decreases and the coulombic efficiency increases naturally. In the 40th cycle, the discharge capacity reduces to 141.9 mAh g^{-1}. Although the theoretical capacity of anatase TiO_2 is 335 mAh g^{-1} [27], the practical achievable capacity is only half of the theoretical capacity, this is mainly because of the fact that, presence of Li greater than $x = 0.5$ in Li_xTiO_2 leads to strong Li–Li interaction in the lattice [28,29].

To probe the electrochemical behavior of TiO_2 hollow sphere electrodes during the cycles, CV measurement was carried out at a scan rate of 0.2 mV s^{-1} after the 10th cycle, which is presented in Fig. 7. The obtained CV profile shows an apparent pair of reduction/oxidation peaks located at 1.695 and 2.086 V (versus Li^+/Li), which are characteristic for Li^+ intercalation/deintercalation reactions in anatase lattice. The interval of cathodic/anodic peaks of the TiO_2 hollow sphere electrode is 0.391 V, much lower than that of

the nanocrystalline TiO_2 (0.49 V) [14]. Because the peak separation is determined by the overpotential required for the transformation of TiO_2 to Li$x$$TiO_2$, the lower peak potential interval indicates that the lithium inserting reaction of TiO_2 hollow spheres is more easily [30,31]. The ratio for anodic (i_{pa}) and cathodic (i_{pc}) peak currents, i_{pa}/i_{pc}, is nearly 1, which demonstrates that Li ions intercalate and deintercalate reversibly and this redox system remains in equilibrium throughout the potential scan [26].

4. Conclusions

Anatase TiO_2 hollow spheres were synthesized successfully by a simple sol–gel process using carbon spheres as template in this work. There were a large initial discharge capacity of 291.2 mAh g^{-1} and a little discharge capacity fading of 1.72 mAh g^{-1} per cycle in the following 39 cycles. CV results exhibited a pair of cathodic/anodic peaks and the peak interval was only 0.391 V when the scan rate was 0.2 mV s^{-1}. It is believed that the short Li diffusion distance, large contact area between TiO_2 and electrolyte, and the well mixing of TiO_2 with AB have enhanced both the efficiency of Li ion and electronic conductivity, hence improving the electrochemical properties.

Acknowledgements

This work has been supported by National Natural Science Foundation of China (Grant No. 60476001) and by the Project of Cultivating Innovative Talents for Colleges & Universities of Henan Province (No. 2002006) and Open Research foundation of Henan University.

References

[1] K.M. Abrham, Electrochim. Acta 38 (1993) 1233.
[2] C. Natarajan, K. Setoguchi, G. Nogami, Electrochim. Acta 43 (1998) 3371.
[3] M. Endo, C. Kim, K. Nishimura, T. Fujino, K. Miyashita, Carbon 38 (2000) 183.
[4] J.J. Auborn, Y.L. Barbero, J. Electrochem. Soc. 134 (1987) 368.
[5] S.Y. Huang, L. Kavan, I. Exnar, M. Grätzel, J. Electrochem. Soc. 142 (1995) L142.
[6] C.H. Jiang, Y. Zhou, I. Honma, T. Kudo, H.S. Zhou, J. Power Sources 166 (2007) 514.
[7] J.Y. Luo, L. Cheng, Y.Y. Xia, Electrochem. Commun. 9 (2007) 1404.
[8] S.Q. Wang, J.Y. Zhang, C.H. Chen, Scripta Mater. 57 (2007) 337.
[9] H.S. Qian, G.F. Lin, Y.X. Zhang, P. Gunawan, R. Xu, Nanotechnology 18 (2007) 355602.
[10] X.X. Li, Y.J. Xiong, L.F. Zou, M.T. Wang, Y. Xie, Micropor. Mesopor. Mater. 112 (2008) 641.
[11] Y.X. Zhang, G.H. Li, Y.C. Wu, T. Xie, Mater. Res. Bull. 40 (2005) 1993.
[12] M.M. Titirici, M. Antonietti, A. Thomas, Chem. Mater. 18 (2006) 3808.
[13] V. Subramanian, A. Karki, K.I. Gnanasekar, F.P. Eddy, B. Rambabu, J. Power Sources 159 (2006) 186.
[14] S.J. Bao, Q.L. Bao, C.M. Li, Z.L. Dong, Electrochem. Commun. 9 (2007) 1233.
[15] J.W. Xu, C.H. Jia, B. Cao, W.F. Zhang, Electrochim. Acta 52 (2007) 8044.
[16] Y.F. Wang, M.Y. Wu, W.F. Zhang, Electrochim. Acta 53 (2008) 7863.
[17] X. Sun, Y. Li, Angew. Chem., Int. Ed. Engl. 43 (2004) 597.
[18] B. Song, S.W. Liu, J.K. Jian, M. Lei, X.J. Wang, H. Li, J.G. Yu, X.L. Chen, J. Power Sources 180 (2008) 869.
[19] J. Li, Y.L. Jin, G.X. Zhang, H. Yang, Solid State Ionics 178 (2007) 1590.
[20] G. Sudant, E. Baudrin, D. Larcher, J.M. Tarascon, J. Mater. Chem. 15 (2005) 1263.
[21] A.N. Jansen, A.J. Kahaian, K.D. Kepler, P.A. Nelson, K. Amine, D.W. Dees, D.R. Vissers, M.M. Thackeray, J. Power Sources 81 (1999) 902.
[22] L. Kavan, M. Gratzel, J. Rathousky, A. Zukal, J. Electrochem. Soc. 143 (1996) 394.
[23] Y.K. Zhou, L. Cao, F.B. Zhang, B.L. He, H.L. Li, J. Electrochem. Soc. 150 (2003) A1246.
[24] Z. Ying, Q. Wan, H. Cao, Z.T. Song, S.L. Feng, Appl. Phys. Lett. 87 (2005) 113108.
[25] J.R. Li, Z.L. Tang, Z.T. Zhang, Electrochem. Solid-State Lett. 8 (2005) A316.
[26] A.R. Armstrong, G. Armstrong, J. Canales, R. García, P.G. Bruce, Adv. Mater. 17 (2005) 862.
[27] L.D. Noailles, C.S. Johnson, J.T. Vaughey, M.M. Thackeray, J. Power Sources 81–82 (1999) 259.
[28] L. Kavan, K. Kratochvilova, M. Gratzel, J. Electroanal. Chem. 394 (1995) 93.
[29] L. Kavan, J. Rathousky, M. Gratzel, V. Shklover, A. Zukal, J. Phys. Chem. B 104 (2000) 12012.
[30] P. Krtil, D. Fattakhova, L. Kavan, S. Burnside, M. Gratzel, Solid State Ionics 135 (2000) 101.
[31] H. Lindstrom, S. Sodergren, A. Solbrand, H. Rensmo, J. Hjelm, A. Hagfeldt, S.E. Lindquist, J. Phys. Chem. B 101 (1997) 7717.